# Phase Decomposition in Blends of Polycarbonate and Isotactic Poly(methyl methacrylate)

**Thein Kyu* and Dong-Soo Lim†**

*Institute of Polymer Engineering, The University of Akron, Akron, Ohio 44325*

*Received August 24, 1990; Revised Manuscript Received January 24, 1991*

ABSTRACT: The dynamics of phase separation and dissolution in a miscible blend of polycarbonate (PC) and isotactic poly(methyl methacrylate) (i-PMMA) has been investigated by means of time-resolved light scattering. The PC/i-PMMA system reveals a reversible lower critical solution temperature (LCST). Several temperature jumps were undertaken from a single phase into an immiscible two-phase region. The time evolution of scattering curves shows no movement of the peak for a considerable period as predicted by the linearized Cahn–Hilliard theory developed for spinodal decomposition. The late stage of phase decomposition follows a power law with an exponent of $^1/_3$ in the growth of fluctuations versus time plots. The kinetic study was extended to the phase dissolution process by conducting temperature quench experiments. The results were analyzed in terms of a simple Fickian diffusion. Finally, the universal scaled curves were compared at the critical compositions of PC/i-PMMA and PC/h-PMMA (heterotactic poly(methyl methacrylate)) to elucidate the influence of tacticity.

## Introduction

Polycarbonate (PC) and poly(methyl methacrylate) (PMMA) have been perceived to be an immiscible pair in earlier works.[1,2] However, this perception has changed recently as PC and heterotactic PMMA (h-PMMA) were found to form a single-phase blend by rapid solvent casting or coagulation.[3-6] These single-phase mixtures are thermodynamically unstable and undergo thermally induced phase separation upon thermal treatment. A cloud point phase diagram, similar to a lower critical solution temperature (LCST), was observed for the PC/h-PMMA blends but is not reversible. The nonreversible character may be due to the strong dependence of the cloud point on the heating rate,[5] in which the cloud point temperatures could be very close to the glass transition temperatures ($T_g$). It was suspected that the strong heating rate dependence of phase separation in PC/h-PMMA blends may be due to the slow diffusion of macromolecules near their $T_g$'s. We thought that if PC/PMMA were truly miscible, it should be identifiable with isotactic PMMA (i-PMMA) because of its low $T_g$ (~50 °C). Moreover, it should be of interest to investigate the influence of tacticity on phase behavior in PC/PMMA blends. This has led to studies on blends of PC with three PMMA isomers.[7]

PC/syndiotactic PMMA (s-PMMA) showed complete miscibility over a considerable range of PMMA molecular weight investigated.[7,8] On the other hand, PC/i-PMMA blends reveal an LCST type cloud point phase diagram and it is reversible.[7] In this article, we present the dynamic aspects of phase separation and dissolution in amorphous PC/i-PMMA blends. Several temperature jump ($T$ jump) and temperature quench ($T$ quench) experiments were performed using time-resolved light scattering to elucidate the dynamics of phase separation. The kinetic results were compared with those obtained for the PC/h-PMMA blends.[9,10]

## Experimental Section

Bisphenol A PC ($M_n$ ~ 30 500 and $M_w/M_n$ ~ 2.1) and isotactic PMMA ($M_n$ ~ 18 000, $M_w/M_n$ ~ 4.2, and i/h/s = 90/4/6) were purchased from Scientific Polymer Products and Polymer Laboratories, respectively. The average molecular weight and polydispersity were determined by gel permeation chromatography (Waters, GPC-150). The tacticity of PMMA was determined by nuclear magnetic resonance (NMR) spectrometry (Varian, Gemini-200) using 5% CDCl solution. Thin blend films (5–25 μm) were cast on glass slides and/or in Petri dishes from 2 wt % tetrahydrofuran solutions. The films were dried in a vacuum oven at 70 °C for at least 72 h and kept in a desiccator prior to use.

A cloud point phase diagram was established by annealing the blends for 2 h at each temperature and examining the cloudy appearance of the films. Rate-dependent cloud points were also determined by a conventional light scattering technique. The dynamic study of phase separation and dissolution was undertaken at the 60/40 PC/i-PMMA composition using time-resolved light scattering. The setup of the light scattering apparatus was described in detail elsewhere.[4] A set of heating blocks were used for $T$ jump and $T$ quench experiments. One was set at experimental temperatures and the other was used for preheating. $T$ jump/quench experiments were carried out by rapidly transferring the specimens from a preset temperature to the experimental temperatures. The time for equilibrating the specimens at the experimental temperatures varies from 30 to 60 s depending on the jump/quench depths. The evolution of scattering intensity profile was monitored through a Vidicon camera (Model 1252B, EG&G Princeton Applied Research Co.), interlinked with an optical multichannel analyzer (OMA III, EG&G). A 5-mW He–Ne laser with a wavelength of 632.8 nm was used as a light source. The temperature was controlled by a PID type temperature controller (Model 2012-P2, Omega Engineering).

## Results and Discussion

**Phase Equilibria.** Figure 1 depicts the cloud point phase diagram for PC/i-PMMA blends obtained by the 2-h annealing test. It reveals an LCST character with a minimum at the 60/40 PC/i-PMMA composition and 212 °C. It is known that the PC/h-PMMA system exhibits a strong heating rate dependence. A similar behavior is expected to occur in the present PC/i-PMMA blends. However, as can be seen in Figure 2, the cloud point at the zero heating rate was estimated to be very close to the phase separation temperature obtained by the 2-h annealing test. It should be emphasized that the process of phase separation in this PC/i-PMMA can be reversed from a two-phase system to a single-phase system by lowering the temperature across the phase boundary. This phase inversion process, known as phase dissolution, permits us to approach the phase boundary from both sides; the observed cloud point by the said approach for 60/40 PC/

* To whom correspondence should be addressed.
† Present address: Hannam Chemical Corp., Ulsan, Korea.

0024-9297/91/2224-3645$02.50/0 

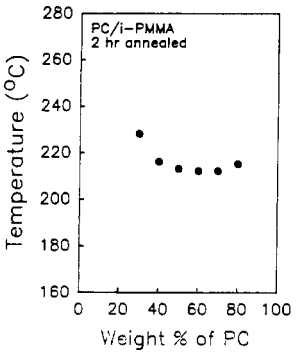


**Figure 1.** Cloud point phase diagram for PC/i-PMMA blends obtained at a heating rate of 2 °C/min.

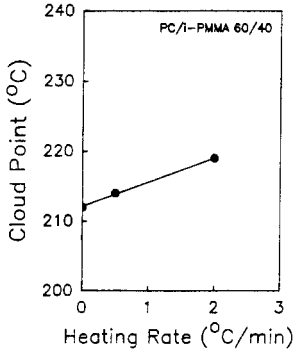


**Figure 2.** Dependence of cloud point on heating rate for the 60/40 PC/i-PMMA blend.

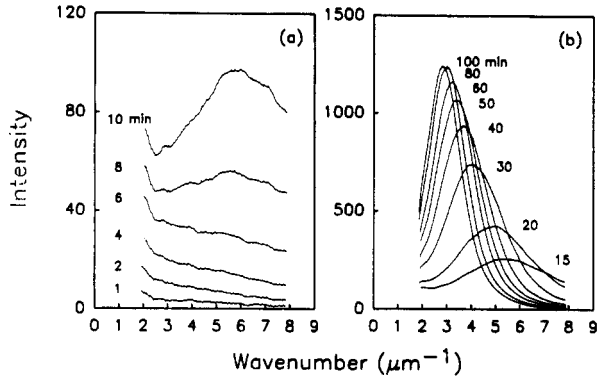


**Figure 3.** Time evolution of scattering curves for the 60/40 PC/i-PMMA composition following a temperature jump from 150 to 220 °C.

i-PMMA is within 1 °C of that obtained at the zero heating rate. Hence, the cloud point phase diagram shown in Figure 1 should be sufficiently close to the coexistence (binodal) curve. In view of the large polydispersity of i-PMMA and PC, the above phase diagram should be regarded only as a pseudo phase diagram.

**Early Stage of Phase Separation.** Three $T$ jumps were undertaken for the 60/40 PC/i-PMMA blends from a single phase (150 °C) into a two-phase region (220, 225, and 228 °C). Figure 3 illustrates the time evolution of scattering profiles for a $T$ jump to 220 °C. Initially, the intensity increases gradually with time without revealing a maximum. Then a scattering peak corresponding to the average periodic distance of phase-separated domains appears and remains stationary for ca. 10 min. Subsequently, the peak moves to a lower scattering wavenumber with elapsed time due to the growth of concentration fluctuations. The invariance of the scattering peak position in the early stage is one of the features predicted by the linearized Cahn–Hilliard (C–H) theory.[11] The deficiency of the linearized theory was pointed out by

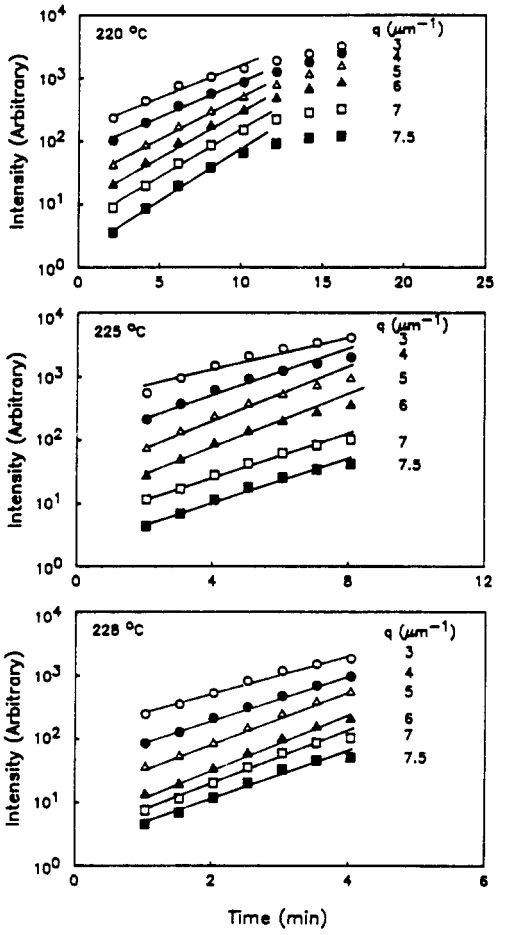


**Figure 4.** Logarithmic intensity versus phase separation time plots obtained at various $T$ jumps.

Cook,[12] who subsequently modified the equation by incorporating thermal fluctuations of a single phase, i.e.

$$S(q,t) = S_s(q) + \{S(q,t=0) - S_s(q)\} \exp[2R(q)t] \quad (1)$$

where $S_s(q) \sim I_s(q)$ and is a virtual structure function of the single phase, i.e., an extrapolated structure factor into a two-phase region assuming analytical continuity in the mean-field approximation.[13,14] The amplification factor $R(q)$ which represents the growth rate of concentration fluctuations may be expressed as

$$R(q) = -Mq^2[\partial f^2/\partial c^2 + 2\kappa q^2] \quad (2)$$

where $q$ is the wavenumber, which is further related to the wavelength of light ($\lambda$) and the scattering angle ($\theta$) by $q = (4\pi/\lambda) \sin(\theta/2)$. $M$ is the Onsager type mobility, $f$ the local free energy density, $c$ the concentration, and $\kappa$ the concentration gradient coefficient. Okada and Han[14] reported that the intensity correction for the thermal fluctuation is crucial when the system is very close to the spinodal point.

Next, the observed intensity was corrected by subtracting the background intensity acquired at the onset of phase separation. Figure 4 depicts plots of the corrected intensity versus phase separation time in semilogarithmic form for various $T$ jumps. For the convenience of comparison, the intensity data were shifted vertically for each wavenumber. It is obvious that the logarithmic intensity shows approximate linear dependence on time in the early stage up to 10 min at 220 °C. These results are in good agreement with the experimental observation (Figure 3), where the peak position is unchanged for 10 min. The amplification factor $R(q)$ can be evaluated from the linear slope in the

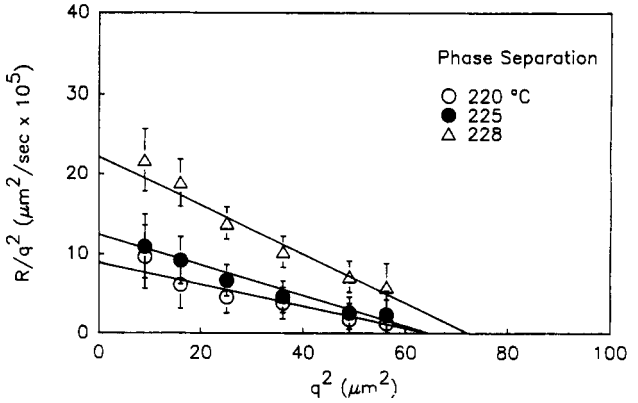


**Figure 5.** Plot of $R(q)/q^2$ versus $q^2$ for the 60/40 PC/i-PMMA mixture at 220, 225, and 228 °C.

early stage. In other $T$ jumps to 225 and 228 °C, a similar trend was observed, but the period for the early stage became shorter at higher $T$ jumps.

To test the applicability of the linearized C–H theory, the $q$ dependence of $R(q)$ has been widely employed. The C–H theory predicts that $R/q^2$ has a linear relationship with $q^2$ as required by eq 2. However, several studies in some polymeric mixtures[15-18] have reported that the plot of $R/q^2$ vs $q^2$ shows a curvature rather than a straight line. This discrepancy has been attributed to the influence of nonlinear terms arising from the growth of concentration fluctuations. In the present case, $R/q^2$ varies approximately linearly with $q^2$ (Figure 5) at smaller $T$ jumps, but the highest $T$ jumps show a tendency toward a smooth curve. The wavenumber maximum for each temperature was estimated to be ca. 6.5 $\mu m^{-1}$ from $R(q)$ versus $q$ plots[10] (not shown here as similar values may be estimated from the initial scattering peak in Figure 2). Linear slopes were drawn in Figure 5 with the aid of the relation

$$q_m^2 = (1/2)q_c^2 \tag{3}$$

where $q_c$ is the crossover wavenumber and $q_m$ the wavenumber maximum. These linear slopes are fairly reasonable, suggesting the applicability of the linearized C–H theory to the early stage of spinodal decomposition. This result is in good accord with those reported for other polymeric blends.[19-22]

The apparent diffusivity $D_{app}$, which is defined as $D_{app} = -M(\partial^2 f/\partial c^2)$, may be determined from the intercept of the plot of $R/q^2$ vs $q^2$ in accordance with eq 2. The values of $D_{app}$ were obtained to be $0.9 \times 10^{-4}$, $1.2 \times 10^{-4}$, and $2.3 \times 10^{-4}$ $\mu m/s^{-1}$ for 220, 225, and 228 °C, respectively. These values are about twice larger than those for the 40/60 PC/h-PMMA blends at the same temperatures ($0.48 \times 10^{-4}$ and $1.2 \times 10^{-4}$ $\mu m/s^{-1}$ at 220 and 228 °C) but at different depths.[10] This result may be a consequence of the higher chain flexibility of i-PMMA or lower $T_g$ relative to that of h-PMMA.[7] The spinodal point, which is defined as the temperature at which the diffusivity becomes zero, is estimated to be 212 °C, and thus is consistent with the cloud point shown in Figure 1. Near the spinodal temperature ($T_s$), $D_{app}$ may be scaled as

$$D_{app} = D_0\epsilon^{\nu} \tag{4}$$

with

$$\epsilon = (T - T_s)/T_s \tag{5}$$

where $D_0$ is the self-diffusion coefficient and $\nu$ is the critical exponent. The value of $\nu$ has been predicted to be unity in the mean-field theory, whereas it is estimated to be 0.63 for solution mixtures by the Ising-like model.[15] Snyder et al.[15] and Hashimoto et al.[19] obtained $\nu = 1$ for polystyrene (PS)/poly(vinyl methyl ether) (PVME) blends. The same exponent was also determined by us for a (hydroxypropyl)-cellulose/water system.[23] As can be seen in Figure 6, we also obtained the slope of unity for this PC/i-PMMA system, which confirms that the mean-field theory is indeed a good approximation for polymer blends.[24,25]

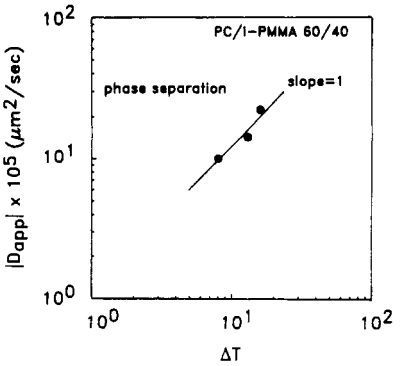


**Figure 6.** log–log plot of $D_{app}$ versus $(T - T_s)$ for the 60/40 PC/i-PMMA blend.

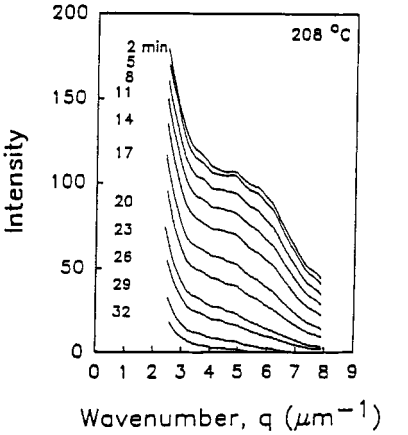


**Figure 7.** Decay of scattering intensity profiles of the 60/40 PC/i-PMMA blend after quenching from 220 to 208 °C.

**Phase Dissolution.** Phase dissolution is a homogenization process of a two-phase structure into a single phase. The criterion of phase dissolution is determined by a stability condition such that the second derivative of free energy is always positive; thus the diffusion is positive. The kinetic study of phase dissolution was undertaken by annealing the single-phase 60/40 PC/i-PMMA blends into the immiscible region (220 °C) for ca. 10 min to ensure that the fluctuation size was sufficiently small. Then the phase-separated blends were quenched below the phase boundary and the time evolution of scattering intensity was monitored at five $T$ quenches (192, 197, 205, 208, and 210 °C). Figure 7 shows the decay of scattering intensity after quenching to 208 °C. The scattering intensity gradually reduces with dissolution time associated with the decay of concentration fluctuations. The blend films became totally transparent after complete dissolution. Differential scanning calorimetry studies of these films show a single $T_g$ for the blends, suggesting the recovery of the homogeneous single-phase blend.

In general, the dissolution is considered to be a simple diffusion process[26] along the concentration gradient which may be treated by a well-known Fick's equation. In this case, the decay rate $-R(q)$ may be expressed as

$$-R(q) = -D_{app}q^2 \tag{6}$$

Figure 8 shows the change of logarithmic intensity as

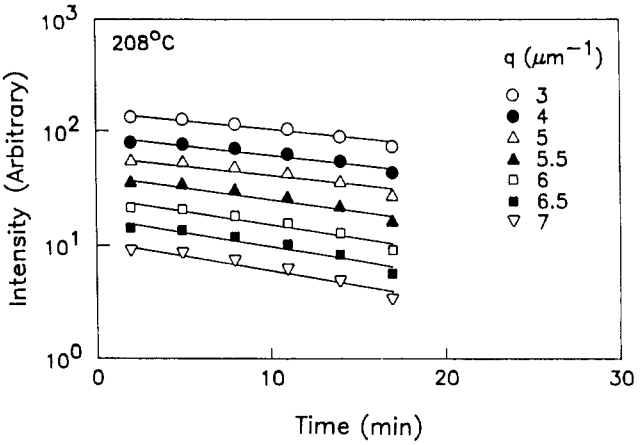


**Figure 8.** Change of logarithmic intensity as a function of dissolution time at 208 °C.

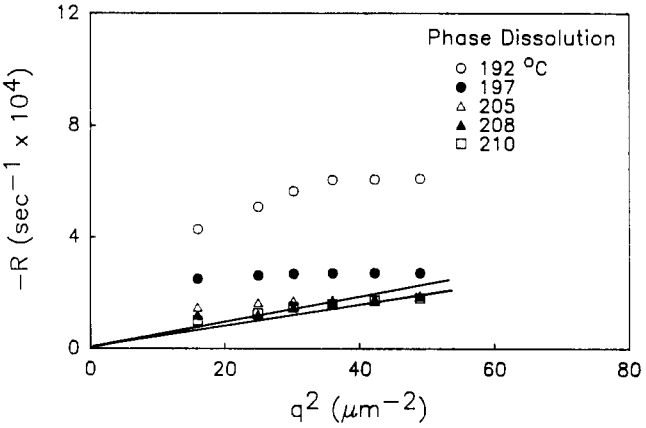


**Figure 9.** Plot of $R(q)$ versus $q^2$ for the phase dissolution of the 60/40 PC/i-PMMA blend.

a function of dissolution time at 208 °C. In every wavenumber, the plots can be approximated by straight lines. The decay rate $-R(q)$ can be obtained from the linear slope according to eq 1. We first applied the Fick model to the dissolution process and plotted $-R(q)$ against $q^2$. As shown in Figure 9, only the scattering data at shallow quenches can be fitted fairly well by a straight line through the origin as implied in eq 6, but at larger quench depths, the data deviate from the origin, indicating the failure of Fick's law. Kumaki and Hashimoto[26] also found that the Fickian diffusion is applicable to the dissolution only when the concentration gradient effect is small.

Alternatively, we tested the applicability of the C–H model to the dissolution process by plotting $-R(q)/q^2$ against $q^2$ as shown in Figure 10. The data at large quench depths show a curvature, suggesting the failure of the linear theory in explaining the phase dissolution. At smaller quench depths, the data can be approximated by straight lines, but $R(q)/q^2$ shows little or no dependence on $q^2$. This in turn suggests that the second term in eq 2 is negligible; i.e., eq 2 reduces to eq 6. In other words, the contribution from the concentration gradient at the interface may be insignificant; thus the $D_{app}$ should be the same as those from the Fick model (eq 6). The apparent diffusivity for the phase dissolution at shallow quenches is shown in Figure 11 as a function of temperature together with the phase separation results. The temperature at which $D_{app}$ becomes zero may be assigned to the spinodal point for the 60/40 PC/i-PMMA composition. The spinodal temperature obtained by interpolation (~212 °C) is quite close to the cloud point (Figure 1). The plot of $D_{app}$ versus $\Delta T = (T - T_s)$ also gives a slope of 1, thus confirming the result of the phase separation process (Figure 6).

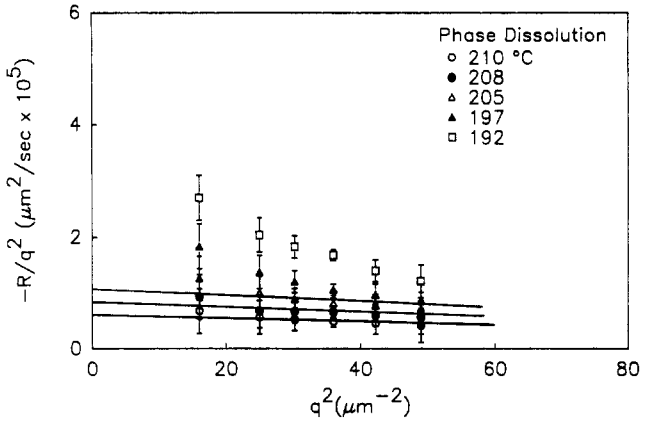


**Figure 10.** Plot of $R(q)/q^2$ against $q^2$ for the phase dissolution of the 60/40 PC/i-PMMA blend.

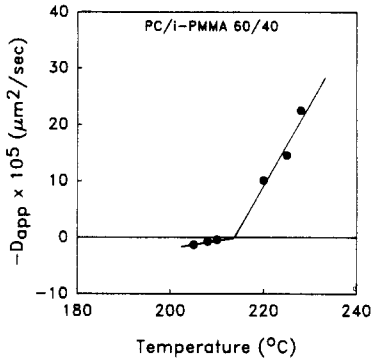


**Figure 11.** Temperature dependence of $D_{app}$ of phase dissolution in comparison with those of phase separation.

**Late Stage of Spinodal Decomposition (SD).** As the phase separation proceeds beyond the early stage of SD, the size of concentration fluctuations becomes significant. The movement of scattering peak to lower scattering angle indicates the growth of concentration fluctuations (Figure 3). The linearized C–H theory is no longer applicable since the higher order terms become dominant in this growth regime. The time dependence of peak position ($q_m$) and scattering maximum ($I_m$) are known to follow the power-law relationships

$$q_m \sim t^{-\phi} \tag{7}$$

and

$$I_m \sim t^{\psi} \tag{8}$$

The exponents $\phi$ and $\psi$ have been extensively investigated theoretically as well as experimentally. One of the most successful theories is that of Langer, Bar-on, and Miller (LBM),[27] which predicts the value of $\phi$ to be $^1/_6$ at the early regime and 0.21 at an intermediate stage. However, it cannot account for the late stages of growth. On the other hand, Binder and Stauffer (BS),[28] based on the coalescence of cluster domains to minimize the surface free energy, reached the relation $\psi = 3\phi$, with $\psi = 1$ and $\phi = ^1/_3$ for the late stages of SD. Later, Binder[29] predicted that the early and intermediate stages may be scaled as $\phi = 1/(d + 3)$ for surface mobility and $\phi = 1/(d + 2)$ for bulk mobility, respectively. Here, $d$ is the dimensionality of growth. The BS prediction for the late stages of SD is the same as the evaporation–condensation model of Lifshift and Slyozov,[30] in which the droplet size grows with an exponent of $^1/_3$. The above models did not take into consideration the hydrodynamic effect, which plays a part in the coalescence of the growing domains in which the suspending components between them must be squeezed

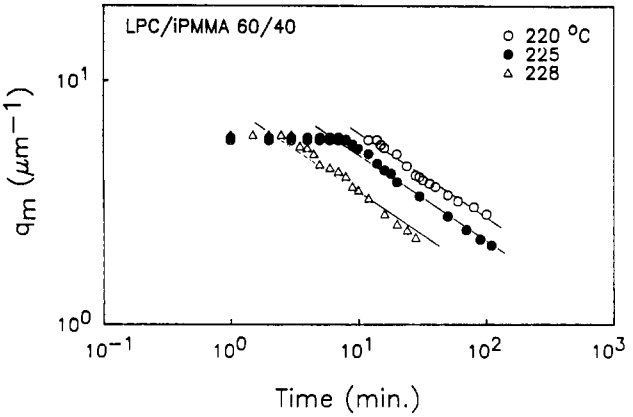


**Figure 12.** Variation of $q_m$ versus phase separation time in double-logarithmic form for the 60/40 PC/i-PMMA blend.

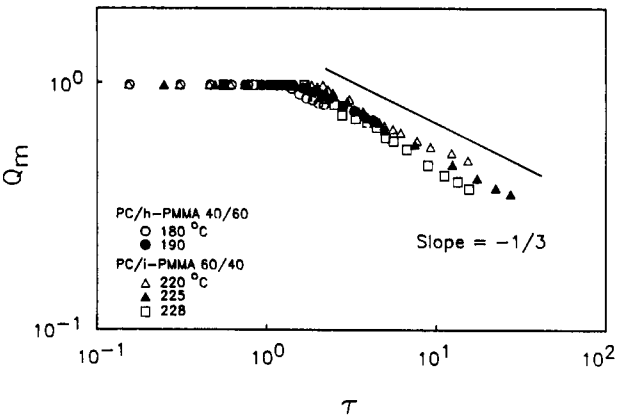


**Figure 13.** Universal curve with reduced variables $Q_m$ versus $\tau$, showing a good superposition with a slope of $-1/3$.

out. Such a phenomenon was incorporated in Siggia's treatment,[31] who arrived at the same equation as BS, but the value of $\phi$ was estimated to be $1/3$ in the early growth regime and it became unity when hydrodynamic flow occurred.

Figure 12 shows the change of $q_m$ as a function of separation time for the 60/40 PC/i-PMMA blend. It was observed that $q_m$ can be scaled with the slopes of $-1/3$ in the late stages. This result is in good agreement with the predictions by various authors mentioned earlier[28,30] and also with the experimental observations in polymer blends,[19-22] including our previous study on the critical composition of the PC/h-PMMA blend.[9,10]

**Scaling Tests.** It seems quite interesting to note that the present results are consistent with those of the PC/h-PMMA blends reported earlier.[10] As mentioned earlier, the diffusivity (or the mobility) of the chains in PC/i-PMMA blends is approximately twice larger than that of PC/h-PMMA blends at the same temperatures (but different $T$ jump depths). To compare both results on the same scale, a universal temporal scaling was performed in terms of reduced variables such as the reduced peak position $Q_m$ and reduced time $\tau$, which may be defined as

$$Q_m = q_m(t)/q_m(0) \tag{9}$$

$$\tau = D_{app} q_m(0)^2 t \tag{10}$$

where $q_m(0)$ is the peak position at $t = 0$, which may be determined by analyzing the early stage of SD or the correlation length in the single phase. Figure 13 illustrates the universal curve showing a good superposition with a slope of $-1/3$ irrespective of the $T$ jump depths or the difference in the stereoregularity of PMMA. These indicate that there is no specific effect of tacticity on the

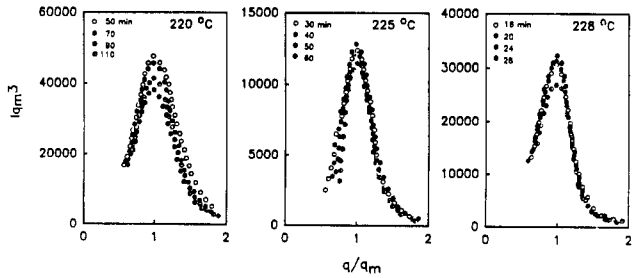


**Figure 14.** Master plots of $I(q,t)q_m^3$ versus $q/q_m$ for the 60/40 PC/i-PMMA blend at late stages of phase separation.

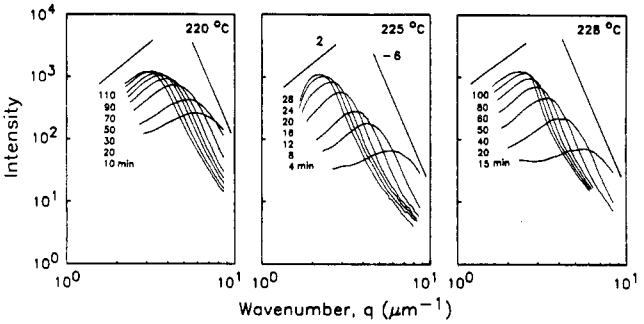


**Figure 15.** Double-logarithmic plots of scattered intensity against wavenumber at various phase separation times for the critical 60/40 PC/i-PMMA composition.

kinetics of phase growth in the late stages of SD. The universal scaling is not only operative for polymer blends but also applicable to other materials such as monomeric liquids, glasses, and metal alloys.[25] The only unique feature with polymeric systems is the molecular weight effect on the universal curve, in which the chain entanglement was shown to retard the domain growth even on the reduced time scale.[32] It should be pointed out that a slight change in polymer configurations does not affect the dynamic behavior of phase decomposition in a universal temporal scaling; however, it exerts a dramatic effect on the miscibility phase diagram.[7]

In the PC/h-PMMA blends, we observed the self-similarity in the late stage of SD where the structure function becomes universal with time. In the present case, it seems useful to carry out the scaling tests for self-similarity[33] and the shape of the structure function[34] for the purpose of comparison between the dissimilar PMMA stereoisomer blends with PC. Figure 14 shows plots of $I(q,t)q_m^3$ versus $q/q_m$ for the late stages of phase separation for 60/40 PC/i-PMMA. As shown in Figure 14, the temporal scaling appears reasonable at longer times in all $T$ jumps, which suggests the self-similarity in the universal regime. This observation is in good agreement with that of PC/h-PMMA.[9,10]

Next, we examined the dynamical scaling of the shape of the structure function by plotting the scattered intensity against scattering wavenumber in the double-logarithmic scale in Figure 15. The shape of the scattering profiles may be scaled as 2 at $q < q_m$ and $-6$ at $q > q_m$ for 60/40 PC/i-PMMA. These exponents are exactly the values predicted theoretically by Furukawa[34] for the critical mixture and are also consistent with our previous observations,[9] where 2 and $-6$ were obtained for the 40/60 PC/h-PMMA critical mixture and 2 and $-4$ for the 70/30 PC/h-PMMA off-critical mixture. The present scaling result suggests that 60/40 PC/i-PMMA may be the near-critical composition. Hence, it may be concluded that the kinetic behavior is the same for the near-critical compositions of the PC/i-PMMA and PC/h-PMMA blends.

## Conclusions

It was demonstrated that PC/i-PMMA exhibits an LCST phase diagram. Unlike the previous PC/h-PMMA blends, we are able to confirm the phase reversibility. Time-resolved light scattering studies on the 60/40 PC/i-PMMA composition revealed that the linearized Cahn–Hilliard theory seems applicable to the early stage of SD. The spinodal point for the 60/40 PC/i-PMMA blend obtained in the kinetic study was found to be very close (within 1 °C) to that of the coexistence temperature. In the late stage of spinodal decomposition, it follows the power law with the exponent of $-1/3$. It was shown that the diffusion coefficients of PC/i-PMMA are nearly twice those of PC/h-PMMA at the same temperatures because of the lower $T_g$ of i-PMMA. However, there is no difference in the kinetic behavior between the near-critical compositions of the PC/i-PMMA and PC/h-PMMA blends when the growth process is reduced to the universal curve.

**Acknowledgment.** Support of this work by the Edison Polymer Innovation Corp. (EPIC) is gratefully acknowledged.

## References and Notes

(1) Gardlund, Z. G. In *Polymer Blends and Composites in Multiphase Systems*; Han, C. D., Ed.; Advances in Chemistry 206; American Chemical Society: Washington, DC, 1984; Chapter 9, p 129.
(2) Koo, K. K.; Inoue, T.; Miyasaka, K. *Polym. Eng. Sci.* **1985**, *27*, 741.
(3) Saldanha, J. M.; Kyu, T. *Macromolecules* **1987**, *20*, 2840.
(4) Kyu, T.; Saldanha, J. M. *J. Polym. Sci., Polym. Lett. Ed.* **1988**, *26*, 33.
(5) Chiou, J. S.; Barlow, J. W.; Paul, D. R. *J. Polym. Sci., Polym. Phys. Ed.* **1987**, *25*, 1459.
(6) Kambour, R. P.; Gundlach, P. E.; Wang, I. C. W.; White, D. M.; Yeager, G. W. *Polym. Prepr. (Am. Chem. Soc., Div. Polym. Chem.)* **1987**, *28*, (2), 140.
(7) Kyu, T.; Lim, D. S. *Chemtracts—Macromol. Chem.* **1990**, *1*, 37.
(8) Kyu, T.; Ko, C. C.; Lim, D. S.; Smith, S.; Noda, I., in preparation.
(9) Lim, D. S.; Kyu, T. *J. Chem. Phys.* **1990**, *92*, 3944, 3951.
(10) Lim, D. S. Ph.D. Dissertation, The University of Akron, Jan 1991.
(11) Cahn, J. W. *J. Chem. Phys.* **1965**, *42*, 93; Cahn, J. W.; Hilliard, J. E. *Ibid.* **1959**, *28*, 258.
(12) Cook, H. E. *Acta Metall.* **1970**, *18*, 297.
(13) Binder, K. *J. Chem. Phys.* **1983**, *79*, 6387.
(14) Okada, M.; Han, C. C. *J. Chem. Phys.* **1986**, *85*, 5317.
(15) Snyder, H. L.; Meakin, P.; Reich, S. *Macromolecules* **1983**, *16*, 757.
(16) Nojima, S.; Nose, T. *Polym. J.* **1982**, *14*, 225, 907.
(17) Rusell, T. P.; Hadziioannou, G.; Warburton, W. K. *Macromolecules* **1985**, *18*, 78.
(18) Hill, R. G.; Tomlins, P. E.; Higgins, J. S. *Macromolecules* **1985**, *18*, 2555.
(19) Hashimoto, T.; Kumaki, J.; Kawai, H. *Macromolecules* **1983**, *16*, 641.
(20) Sato, T.; Han, C. C. *J. Chem. Phys.* **1988**, *88*, 2057.
(21) Bates, F. S.; Wiltius, P. *J. Chem. Phys.* **1989**, *91*, 3285.
(22) Kyu, T.; Saldanha, J. M. *Macromolecules* **1988**, *21*, 1021.
(23) Kyu, T.; Mukherjee, P. *Liq. Cryst.* **1988**, *3*, 631.
(24) de Gennes, P.-G. *J. Chem. Phys.* **1980**, *72*, 4756.
(25) Snyder, H. L.; Meakin, P. *J. Chem. Phys.* **1985**, *73*, 217.
(26) Kumaki, J.; Hashimoto, T. *Macromolecules* **1986**, *19*, 763.
(27) Langer, J. S.; Bar-on, M.; Miller, H. D. *Phys. Rev. A* **1975**, *11*, 1417.
(28) Binder, K.; Stauffer, D. *Phys. Rev. Lett.* **1975**, *33*, 1006.
(29) Binder, K. *Phys. Rev. B* **1977**, *15*, 4425.
(30) Lifshift, I. M.; Slyozov, V. V. *J. Chem. Solids* **1961**, *19*, 35.
(31) Siggia, E. D. *Phys. Rev. A* **1979**, *20*, 595.
(32) Hashimoto, T.; Itakura, M.; Hasegawa, H. *J. Chem. Phys.* **1986**, *85*, 6118.
(33) Furukawa, H. *Phys. Rev. Lett.* **1979**, *43*, 136.
(34) Furukawa, H. *Physica A* **1984**, *123*, 497.

**Registry No.** iPMMA, 25188-98-1; (bisphenol A)(PC) (copolymer), 25037-45-0; (bisphenol A)(PC) (SRU), 24936-68-3.